Inorganic Chemistry

Article

pubs.acs.org/IC

# Structure and Properties of the Precursor/Successor Complex and Transition State of the $CrCl^{2+}/Cr^{2+}$ Electron Self-Exchange Reaction via the Inner-Sphere Pathway

François P. Rotzinger*

Institut des Sciences et Ingénierie Chimiques, Ecole Polytechnique Fédérale de Lausanne (EPFL), Station 6, CH-1015 Lausanne, Switzerland

Supporting Information

**ABSTRACT:** The electron self-exchange reaction $\mathbf{Cr}Cl(OH_2)_5^{2+} + Cr(OH_2)_6^{2+} \rightarrow \mathbf{Cr}(OH_2)_6^{2+} + CrCl(OH_2)_5^{2+}$, proceeding via the inner-sphere pathway, was investigated with quantum-chemical methods. Geometry and vibrational frequencies of the precursor/successor (P/S) complex, $(H_2O)_5Cr^{III}ClCr^{II}(OH_2)_5^{4+}/(H_2O)_5Cr^{II}ClCr^{III}(OH_2)_5^{4+}$, and the transition state (TS), $(H_2O)_5CrClCr(OH_2)_5^{4+\ddagger}$, were computed with density functional theory (DFT) and conductor polarizable continuum model hydration. Consistent data were obtained solely with long-range-corrected functionals, whereby in this study, LC-BOP was used. Bent and linear structures were computed for the TS and P/S. The electronic coupling matrix element ($H_{ab}$) and the reorganizational energy ($\lambda$) were calculated with multistate extended general multiconfiguration quasi-degenerate second-order perturbation theory. The nuclear tunneling factor ($\Gamma_n$), the nuclear frequency factor ($\nu_n$), the electronic frequency factor ($\nu_{el}$), the electron transmission coefficient ($\kappa_{el}$), and the first-order rate constant ($k_{et}$) for the electron-transfer step (the conversion of the precursor complex into the successor complex) were calculated based on the imaginary frequency ($\nu^{\ddagger}$) of the TS, the Gibbs activation energy ($\Delta G^{\ddagger}$), $H_{ab}$, and $\lambda$. The formation of the precursor complex via water substitution at $Cr(OH_2)_6^{2+}$ was also investigated with DFT and found to be very fast. Thus, the electron-transfer step is rate-determining. For the substitution reaction, only a bent TS structure could be obtained. The overall rate constant ($k$) was estimated as the product $K_A k_{et}$, whereby $K_A$ is the equilibrium constant for the formation of the ion aggregate of the reactants $Cr(OH_2)_6^{2+}$ and $CrCl(OH_2)_5^{2+}$, $Cr(H_2O)_6{\cdot}CrCl(OH_2)_5^{4+}$ (IAR). $k$ calculated for the bent and linear isomers agrees with the experimental value.

$$\mathbf{Cr}Cl(OH_2)_5^{2+} + Cr(OH_2)_6^{2+} \xrightarrow{k} \mathbf{Cr}(OH_2)_6^{2+} + CrCl(OH_2)_5^{2+}$$

$$k_{et} = \Gamma_n \nu_n \kappa_{el} e^{-\Delta G^{\ddagger}/RT}$$

$$k = K_A k_{et}$$

$k_{et} = 10-330\ s^{-1}$ at 0°C

$k = 0.3-12\ M^{-1}s^{-1}$ at 0°C and $I = 1$ M

$k(\exp) = 8.3\pm2.0,\ 9.1\pm1.0\ M^{-1}s^{-1}$ at 0°C and $I = 1$ M

## INTRODUCTION

In the early 1950s, Taube and co-workers discovered that electron-transfer reactions can proceed via two different mechanisms called the "inner-sphere" and "outer-sphere" pathways.[1−3] The electron self-exchange reaction (eqs 1 and 2), for which the driving force is zero, is the simplest electron-transfer process. The first self-exchange rates of transition-metal aqua ions, $M(OH_2)_6^{3+}/M(OH_2)_6^{2+}$ and $MX(OH_2)_5^{2+}/M(OH_2)_6^{2+}$ couples [reactions (1) and (2), respectively, with M = V, Cr, Fe, Co and X = OH], have also been measured in the 1950s.[4−13] For the extensively studied $Cr^{II/III}$ and $Fe^{II/III}$ couples, other bridging ligands (X) like F, Cl, Br, $N_3$, and NCS have been investigated as well.[14]

$$\mathbf{M}(OH_2)_6^{3+} + M(OH_2)_6^{2+} \rightarrow \mathbf{M}(OH_2)_6^{2+} + M(OH_2)_6^{3+} \quad (1)$$

$$\mathbf{M}X(OH_2)_5^{2+} + M(OH_2)_6^{2+} \rightarrow \mathbf{M}(OH_2)_6^{2+} + MX(OH_2)_5^{2+} \quad (2)$$

A few years later, Marcus,[15] Hush,[16] and Levich et al.[17] published the nowadays widely used theory for electron transfer. During the following years, this theory was elaborated further by Marcus, Newton, and Sutin et al., and Jortner et al.[18−27]

In the present study, the electron-transfer step (3), the transformation of the precursor (P) complex, $(H_2O)_5Cr^{III}ClCr^{II}(OH_2)_5^{4+}$, into the successor (S) complex, $(H_2O)_5Cr^{II}ClCr^{III}(OH_2)_5^{4+}$, and the substitution reaction at $Cr(OH_2)_6^{2+}$ by $CrCl(OH_2)_5^{2+}$ were investigated with density functional theory (DFT) and wave function theory (WFT). Hence, the rate constant for self-exchange reaction (4) was obtained.

$$(H_2O)_5\mathbf{Cr^{III}}ClCr^{II}(OH_2)_5^{4+} \rightarrow (H_2O)_5\mathbf{Cr^{II}}ClCr^{III}(OH_2)_5^{4+} \quad (3)$$

$$\mathbf{Cr}Cl(OH_2)_5^{2+} + Cr(OH_2)_6^{2+} \rightarrow \mathbf{Cr}(OH_2)_6^{2+} + CrCl(OH_2)_5^{2+} \quad (4)$$

Geometries and vibrational frequencies of the precursor/successor (P/S) complex and the transition state (TS), $(H_2O)_5CrClCr(OH_2)_5^{4+\ddagger}$, as well as their adiabatic energies

**Received:** July 3, 2014
**Published:** August 27, 2014

   dx.doi.org/10.1021/ic5015785 | Inorg. Chem. 2014, 53, 9923−9931

were computed. On the basis of these total energies, the electronic coupling matrix element ($H_{ab}$), the reorganizational energy ($\lambda$), and the Gibbs activation energy ($\Delta G^{\ddagger}$) were calculated. The nuclear frequency factor ($\nu_n$) was estimated from the imaginary mode of the TS. The electronic frequency factor ($\nu_{el}$) was obtained from $H_{ab}$ and $\lambda$ and the electronic transmission coefficient ($\kappa_{el}$) from $\nu_n$ and $\nu_{el}$, and the nuclear tunneling factor ($\Gamma_n$) was available via $\nu_n$ and $\Delta G^{\ddagger}$. On the basis of these data, the rate constant ($k_{et}$) for self-exchange reaction (3) was estimated.

The calculation of the (overall) rate constant of reaction (4) requires the equilibrium constant ($K_A$) for the formation of the ion-aggregate $Cr(OH_2)_6{\cdot}CrCl(OH_2)_5^{4+}$ (IAR) of the reactants $Cr(OH_2)_6^{2+}$ and $CrCl(OH_2)_5^{2+}$ (eq 5), which was estimated based on Fuoss' equation,[28] and the rate constant ($k_{sub}$) for the formation of P from the IAR via water substitution at $Cr(OH_2)_6^{2+}$ by $CrCl(OH_2)_5^{2+}$ (eq 6).

$$Cr(OH_2)_6^{2+} + CrCl(OH_2)_5^{2+} \rightleftarrows Cr(OH_2)_6{\cdot}CrCl(OH_2)_5^{4+} \quad (5)$$

$$Cr(OH_2)_6{\cdot}CrCl(OH_2)_5^{4+} \rightleftarrows (H_2O)_5Cr^{III}ClCr^{II}(OH_2)_5^{4+} + H_2O \quad (6)$$

Reaction (6) was investigated with DFT, and $k_{sub}$ was found to be much faster than $k_{et}$. Because the electron-transfer step is rate-determining, the rate constant ($k$) of reaction (4) was estimated as $K_A k_{et}$.

## COMPUTATIONAL DETAILS

Calculations were performed using the *GAMESS*[29,30] programs. Karlsruhe def2-SV(P), def2-SVP, and def2-TZVP basis sets,[31−33] modified as described in the Supporting Information (SI) and denoted as sv(p), svp, and tzvp, were used. Figures 2, 4, 5, and S1 and S2 in the SI were generated with *MacMolPlt*.[34]

All of the computations were performed for the high-spin state ($S$ = 3.5). For the complete active space (CASSCF) and the multiconfiguration self-consistent-field calculations (MCSCF), a (7/10) active space was used. It contained all 3d molecular orbitals (MOs) of chromium.

Computations on the P/S at the two- or four-state-averaged CASSCF(7/10) level would require the treatment of up to about 20 states, whereby only two or four of them are relevant. The first two states in $(H_2O)_5Cr^{III}ClCr^{II}(OH_2)_5^{4+}$ are nearly degenerate with the $d_{z^2}$- or $d_{x^2-y^2}$-like $d_\sigma$* MOs of $Cr^{II}$ populated. They are needed for the computation of $E_{in,a}$. The other two states of interest, also nearly degenerate, are required for the calculation of $E_{in,b}$. The latter arise from the transfer of the $d_\sigma$* electron of $Cr^{II}$ into the $d_{z^2}$- or $d_{x^2-y^2}$-like $d_\sigma$* MOs of $Cr^{III}$. $E_{in,a}$ and $E_{in,b}$ are used for the computation of $\lambda_{in}$. The additional states stem from one- and two-electron d−d excitations on $Cr^{II}$ and $Cr^{III}$. They were not taken into account because they do not belong to the potential energy surfaces (PESs) being relevant for the electron-transfer reaction (Figure 1). The positions of these states change in the course of the CASSCF iterations. Such computations are very difficult, if not impossible, to converge. With the occupation-restricted multiple active space (ORMAS) technique,[35] the $d_\pi(t_{2g}$-like) electrons were not allowed to be displaced into the $d_\sigma$* MOs, which eliminated the undesired d−d excitations and made the convergence of the two- or four-state-averaged MCSCF computations feasible. The two-ORMAS space MCSCF wave function involved one active space with six electrons in six $d_\pi$ MOs, 6/6, and a second active space with one electron in four $d_\sigma$* MOs, 1/4. It is abbreviated as MCSCF(6/6,1/4,7), whereby "7" is the total number of electrons in the active space. 4st-MCSCF(5−6/6,1−2/4,7), for example, would be a four-state-averaged MCSCF wave function with five to six electrons in the first active space of six MOs and one to two electrons in the second active space of four MOs, including thus excitations of one $d_\pi$ electron into $d_\sigma$* MOs. Dynamic correlation was treated with second-order perturbation theory (PT2) based on CASSCF or MCSCF wave functions using the extended general multiconfiguration quasi-degenerate second-order perturbation (XGMC-QDPT2) method.[36−40] The 3s and 3p MOs of chromium were included in the PT2 treatment.

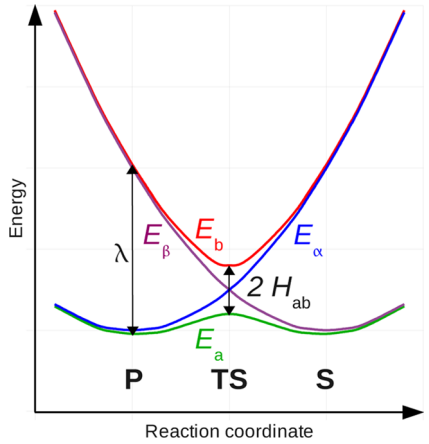


**Figure 1.** Plots of the adiabatic ($E_a$ and $E_b$) and diabatic ($E_\alpha$ and $E_\beta$) energies of an electron self-exchange reaction.

Hydration was treated using the conductor polarizable continuum model (CPCM).[41−43] The cavity was constructed based on Batsanov's[44] van der Waals radii of the atoms. Because of the high charge of these complexes, a finer tessellation than the default had to be used (NTSALL = 960; the respective default is 60). The hydration energies were computed with DFT and MCSCF using 4st-MCSCF(6/6,1/4,7) for the TS and 2st-MCSCF(6/6,1/2,7) for the P/S (equal results were obtained with 2st-MCSCF(6/6,1/2,7)−2st-MCSCF(6/6,1/2,7) and 2st-MCSCF(6/6,1/2,7)−ROHF for TS−P/S). Geometries and vibrational frequencies were computed for the hydrated systems with spin-unrestricted DFT using a grid finer (NRAD = 180 and NLEB = 974) than the default (NRAD = 96 and NLEB = 302). For the TSs and P/Ss, $\langle S^2\rangle$ was 15.82−15.84 and 15.77, respectively. The Hessians were calculated numerically (based on analytical gradients) using the double-difference method and projected to eliminate rotational and translational contaminants.[45] Energies including state−state interactions were computed with multistate extended GMC-QDPT2 (XGMC-QDPT2, using kxgmc=.t., krot=.t., kszdoe=.t., and thrde=0).[40]

The TSs were located by maximizing the energy along the reaction coordinate (the imaginary mode) via eigenmode following. Selected atomic coordinates of the investigated species are given in Tables S1−S5 in the SI.

## RESULTS AND DISCUSSION

**Theoretical Basis.** The PES for the electron self-exchange reaction (3), the transformation of the P complex into the S complex, is depicted in Figure 1.[24] The diabatic energies are denoted by $E_\alpha$ and $E_\beta$, whereas $E_a$ and $E_b$ represent the adiabatic energies, computed including state−state interactions. The Marcus theory is based on the diabatic PESs, which are computationally available via appropriate techniques.[46−49] In the present study, adiabatic PESs were investigated and all of the calculated properties are derived thereof. Thus, computed $\lambda$ values, for example, are only approximations to $\lambda$, as defined by Marcus. The electronic coupling matrix element ($H_{ab}$) is determined (eq 7) by the splitting of the two adiabatic PESs at the TS. Because the hydration energy of the two states is expected to be equal in a good approximation, the second expression of eq 7 was used for the determination of $H_{ab}$ ($E_{in,b}^{\ddagger}$


dx.doi.org/10.1021/ic5015785 | *Inorg. Chem.* 2014, 53, 9923−9931

and $E_{in,a}^{\ddagger}$ represent the adiabatic internal electronic energies of the two states, whereby $E_{in,a}^{\ddagger}$ is abbreviated as $E_{in}^{\ddagger}$).

$$H_{ab} = \frac{1}{2}(E_b^{\ddagger} - E_a^{\ddagger}) \approx \frac{1}{2}(E_{in,b}^{\ddagger} - E_{in,a}^{\ddagger}) \quad (7)$$

The reorganizational energy ($\lambda$) is composed (eq 8a) of the "internal" (solute) reorganizational energy ($\lambda_{in}$) and the "outer-sphere" (solvent) reorganizational energy ($\lambda_{ou}$).

$$\lambda = \lambda_{in} + \lambda_{ou} \quad (8a)$$

$$\lambda_{in} = E_{in,b} - E_{in,a} \quad (8b)$$

$\lambda_{in}$ (eq 8b, whereby $E_{in,a}$ may be abbreviated as $E_{in}$) was calculated as the difference of the gas-phase electronic energies of states a and b (Figure 1) at the geometry of P (or S). As was already mentioned, this is an approximation because, in the Marcus theory, $\lambda$ is based on the difference of the corresponding diabatic energies. $\lambda_{ou}$ can be estimated based on the two-sphere model (eq 9),[16,50−52] whereby $r$ (Table S6 in the SI) represents the Cr···Cr distance in the P/S and $r_{II}$ and $r_{III}$ (Table S6 in the SI) are the radii of the respective $Cr^{II}$ and $Cr^{III}$ fragments of the P/S, estimated as described in the SI. Equation 9 was derived[50−52] by Marcus for outer-sphere electron-transfer reactions. It is based on the assumptions that (i) the electronic donor−acceptor interaction in the TS is weak, (ii) the donor−acceptor distance is constant during the electron-transfer step, and (iii) $r \geq r_{II} + r_{III}$. Items i and iii are valid at least approximately for outer-sphere reactions, but not for inner-sphere reactions, where $H_{ab}$ is large and $r < r_{II} + r_{III}$ (Table S6 in the SI). For inner-sphere reaction (3) involving bent P, TS, and S species, the Cr···Cr distance diminishes by 0.05−0.08 Å upon activation, whereas for the corresponding linear structures, the Cr···Cr reduction amounts to 0.37−0.40 Å. For this latter case, eq 9 is likely to be invalid.

$$\lambda_{ou} = (\Delta e)^2\left(\frac{1}{n^2} - \frac{1}{\varepsilon}\right)\left(\frac{1}{2r_{II}} + \frac{1}{2r_{III}} - \frac{1}{r}\right) \quad (9)$$

$$(\Delta e)^2\left(\frac{1}{n^2} - \frac{1}{\varepsilon}\right) = 753.12 \text{ kJ Å mol}^{-1} \text{ (for water)}$$

Alternatively, $\lambda_{ou}$ can be calculated based on the hydration energies of the TS and P/S (eq 10), whereby $G_{solv}$(TS) and $G_{solv}$(P/S) are the (equilibrium) solvation energies of both the TS and P/S, respectively. Equation 10 is different from eq 9 because the latter is based on the equilibration of solely the nuclear degrees of freedom of the solvent with the TS (and the equilibration of both the electronic and nuclear components of the solvent with the P/S).

$$\lambda_{ou} = 4[G_{solv}(TS) - G_{solv}(P/S)] = 4\Delta G_{solv}^{\ddagger} \quad (10)$$

The electronic activation energy ($\Delta E^{\ddagger}$) for reaction (3) is available from eq 11, whereby $E_{in}^{\ddagger}$ and $E_{in}$ (equal to $E_{in,a}^{\ddagger}$ and $E_{in,a}$, respectively) represent the internal electronic (gas-phase) energies of the TS and P/S, respectively, and $\lambda_{ou}$ is available via eq 9 or 10.

$$\Delta E^{\ddagger} = E_{in}^{\ddagger} - E_{in} + \lambda_{ou}/4 = \Delta E_{in}^{\ddagger} + \lambda_{ou}/4 \quad (11)$$

For adiabatic self-exchange reactions, the activation energy ($\Delta E^{\ddagger}$) can also be determined by eq 12.[23,24]

$$\Delta E^{\ddagger} = \frac{(\lambda/2 - H_{ab})^2}{\lambda} \quad (12)$$

The thermodynamic values $\Delta H^{\ddagger}$, $\Delta S^{\ddagger}$, and $\Delta G^{\ddagger}$ were based on zero-point energies and partition functions for the hydrated species.

From $H_{ab}$ and $\lambda$, the electronic frequency factor ($\nu_{el}$) and the electron transmission coefficient ($\kappa_{el}$) are available (eqs 13 and 14).[19,20] $h$, $N_A$, $R$, and $T$ respectively denote Planck's constant, Avogadro's number, the gas constant, and the absolute temperature.

$$\nu_{el} = \frac{2H_{ab}^{\ 2}}{hN_A}\sqrt{\frac{\pi^3}{\lambda RT}} \quad (13)$$

$$\kappa_{el} = \frac{2(1 - e^{-\nu_{el}/2\nu_n})}{2 - e^{-\nu_{el}/2\nu_n}} \quad (14)$$

In the pertinent literature, the nuclear frequency factor ($\nu_n$) is a real number. For the estimation of $\nu_n$, the corresponding vibrational mode of the bulk solvent ($\nu_{ou}$ = 30 $cm^{-1}$) may be taken into account (eq 15).[18−20] $\nu_{in}$ and $\nu_{ou}$ are the nuclear frequency factors of the solute ("internal") and the solvent ("outer-sphere"). $\nu_{in}$ can be estimated[20] via eq 16, whereby, typically, totally symmetric metal−ligand stretching frequencies of the oxidant and the reductant are taken as $\nu_i$.[18]

$$\nu_n = \sqrt{\frac{\nu_{in}^{\ 2}\lambda_{in} + \nu_{ou}^{\ 2}\lambda_{ou}}{\lambda_{in} + \lambda_{ou}}} \quad (15)$$

$$\nu_{in} = \sqrt{\frac{\sum_i \nu_i^{\ 2} E_i}{\sum_i E_i}} \quad (16)$$

The imaginary mode ($\nu^{\ddagger}$) of the TS (Figure 2) describes the asymmetric displacement of $Cl^-$ and symmetric Cr−O modes. This normal mode resembles the combination of the $Cr^{II}$−O, $Cr^{III}$−O, $Cr^{II}$−Cl, and $Cr^{III}$−Cl modes of the P/S, which would be used in eq 16. $\nu^{\ddagger}$ is the mode transforming the TS into the S (or P), in contrast to $\nu_{in}$ in eq 16 representing the effective mode for the conversion of P into the TS. Hence, $\nu_{in}$ is

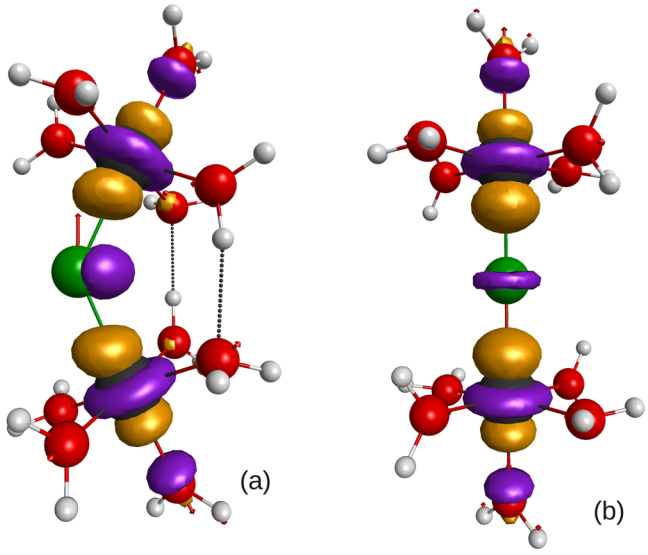


**Figure 2.** Structure of the bent (a) and linear (b) TS with imaginary mode (reaction coordinate) and MO of the electron being transferred [LC-BOP($\mu$=0.33)-CPCM/tzvp calculation]. The chromium, chlorine, oxygen, and hydrogen atoms are represented in black, green, red, and gray and the MOs in purple/gold.


dx.doi.org/10.1021/ic5015785 | Inorg. Chem. 2014, 53, 9923−9931

Table 1. Imaginary Mode ($\nu^{\ddagger}$), Selected Bond Lengths and Angle of the Transition State $(H_2O)_5CrClCr(OH_2)_5^{4+\ddagger}$

| | metal−ligand bond lengths, Å | | | | | |
|---|---|---|---|---|---|---|
| functional/basis set | Cr−Cl | Cr−$O_{ax}$ | Cr−$O_{eq}$ | $d$(Cr···Cr), Å | ∠(Cr−Cl−Cr), deg | $\nu^{\ddagger}$, $cm^{-1}$ |
| | | | (i) Bent TS Structure (CPCM Hydration) | | | |
| LC-BOP/sv(p) | 2.398, 2.398 | 2.102, 2.101 | 1.991−2.098 | 4.308 | 127.9 | 568i |
| LC-BOP/svp | 2.395, 2.394 | 2.103, 2.102 | 1.990−2.090 | 4.333 | 129.6 | 582i |
| LC-BOP/tzvp | 2.396, 2.394 | 2.115, 2.116 | 1.997−2.087 | 4.369 | 131.5 | 627i |
| | | | (ii) Linear TS Structure (CPCM Hydration) | | | |
| LC-BOP/tzvp | 2.414, 2.414 | 2.120, 2.119 | 2.001−2.010 | 4.828 | 179.6 | 460i |
| LC-BOP($\mu$=0.37)/tzvp | 2.415, 2.415 | 2.123, 2.122 | 2.002−2.010 | 4.830 | 179.7 | 628i |
| | | | (iii) Linear TS Structure (Gas Phase) | | | |
| MCSCF/sv(p) | 2.617, 2.617 | 2.208, 2.208 | 2.091−2.098 | 5.235 | 180.0 | 552i |
| LC-BOP/tzvp | 2.559, 2.559 | 2.170, 2.170 | 2.025−2.030 | 5.117 | 180.0 | 318i |
| LC-BOP/sv(p) | 2.556, 2.556 | 2.154, 2.154 | 2.022−2.026 | 5.111 | 180.0 | 298i |
| LC-BOP($\mu$=0.37)/tzvp | 2.562, 2.561 | 2.174, 2.174 | 2.027−2.031 | 5.123 | 180.0 | 389i |
| LC-BOP($\mu$=0.37)/sv(p) | 2.559, 2.559 | 2.158, 2.158 | 2.025−2.029 | 5.118 | 180.0 | 354i |

approximated by the absolute (real) value of the imaginary mode ($\nu^{\ddagger}$) of the TS (the reaction coordinate). Because $\nu^{\ddagger}$ was computed for the hydrated systems, its absolute value might correspond approximately to $\nu_n$; solvent effects on the solute are taken into account, but solvent modes and their coupling with those of the solute are neglected. The nuclear tunneling factor ($\Gamma_n$) was calculated via Skodje and Truhlar's equation (17),[53] whereby $k_B$ is Boltzmann's constant.

$$\alpha = \frac{2\pi}{h\nu_n}, \quad \beta = \frac{1}{k_B T} \tag{17a}$$

$$\Gamma_n = \frac{\beta\pi/\alpha}{\sin(\beta\pi/\alpha)} - \frac{\beta}{\alpha - \beta} e^{(\beta-\alpha)\Delta G^{\ddagger}} \quad (\text{valid for } \beta \le \alpha) \tag{17b}$$

The rate constant for the electron-transfer step ($k_{et}$) is given by eq 18.[18,19]

$$k_{et} = \Gamma_n \nu_n \kappa_{el} e^{-\Delta G^{\ddagger}/RT} \tag{18}$$

**Validation of the Computational Methods.** The geometry optimizations and frequency computations for the hydrated species were performed with DFT. The accuracy of these geometries and frequencies cannot be assessed with high-level WFT, in the present case XGMC-QDPT2, which is only available for electronic energies. Thus, the adequacy of the functionals and basis sets was assessed on the basis of the electronic activation energies ($\Delta E^{\ddagger}$) for self-exchange reaction (3) in comparison with XGMC-QDPT2. Furthermore, $\Delta E^{\ddagger}$ was calculated based on both eqs 11 and 12.

**Transition State $(H_2O)_5CrClCr(OH_2)_5^{4+\ddagger}$.** For the TS and the P/S complexes, a bent and a linear structure exist. The geometry of the bent TS was optimized with CPCM hydration using the LC-BOP[54] functional with the default parameter ($\mu$ = 0.33) for the long-range correction scheme. In LC-DFT, the self-interaction error is reduced by using Hartree−Fock (HF) exchange at large electron−electron distances and DFT exchange at short electron−electron distances, whereby partitioning of these two exchanges is achieved using the erf($\mu r$)/$r$ function for the weight of the HF exchange and erfc($\mu r$)/$r$ for the weight of the DFT exchange ($r$ is the electron−electron separation). This TS has approximately $C_2$ symmetry (Figure 2a). The $p_\sigma$ MO of Cl is $\sigma$*-antibonding with respect to the $d_\sigma$* MOs. The $C_2$ symmetry is only approximate because of numerical inaccuracies, which are favored by the fact that CPCM calculations with *GAMESS* have to be performed in $C_1$ symmetry. Its bent structure gives rise to two hydrogen bonds between equatorial water ligands. With increasing quality of the basis set, the Cr···Cr distance, the Cr−Cl−Cr angle, and the imaginary frequency increase (Table 1). Computations with a larger parameter for the long-range correction ($\mu$ = 0.37) starting from the (bent) LC-BOP/tzvp structure lead to a linear isomer (Figure 2b). In this structure, hydrogen bonds are absent. The geometry is insensitive to $\mu$ but not $\nu^{\ddagger}$ (Table 1), with the latter being considerably smaller for the linear isomer (see LC-BOP/tzvp data).

For both isomers of the hydrated TS, the imaginary mode (Table 1) represents mainly the asymmetric Cr−Cl−Cr and Cr−O(axial) stretches (Figure 2). This frequency is higher than that of any of the $Cr^{II}$−Cl, $Cr^{II}$−O(axial), $Cr^{III}$−Cl, and $Cr^{III}$−O(axial) stretching modes in the corresponding P/S. With HF as well as the corresponding single-configuration-based post-HF methods like MP2 or CI, a broken-symmetry wave function is obtained. Already more than 30 years ago, Logan and Newton[55] observed symmetry breaking for the $Fe(OH_2)_6^{3+}$/$Fe(OH_2)_6^{2+}$ couple at the HF level. This is also seen for many functionals, whereby the long-range-corrected ones are among the few functionals that do not produce broken-symmetry MOs (for the symmetric TS species). Symmetry breaking is also seen with single-state MCSCF, whereas its multistate variant allows the computation of symmetric MOs, provided that state averaging is performed for at least the a and b states (Figure 1). State-specific analytical gradients of multistate MCSCF wave functions are available at the gas-phase level. Starting from the bent hydrated TS structure, the saddle point was recomputed based on the gradient of the first state of the 4st-MCSCF *gas-phase* wave function. The bent structure became linear (Table 1). Also, gas-phase LC-BOP($\mu$=0.33) calculations yielded solely the linear isomer (Table 1). $\nu^{\ddagger}$ augments with increasing $\mu$. The Cr−Cl bonds are considerably longer without hydration, and so is, therefore, also the Cr···Cr distance. At the 4st-MCSCF level, $\nu^{\ddagger}$ is much larger than that with LC-BOP in spite of the weaker Cr−Cl bonds. However, it should be noted that dynamic correlation is neglected. Hence, $\nu^{\ddagger}$ is likely to be overestimated (by ∼10%) with 4st-MCSCF. On the other hand, hydration leads to a substantial increase of $\nu^{\ddagger}$ by ∼50% (LC-BOP/tzvp data in Table 1 for the linear isomer). These data suggest that LC-BOP might underestimate $\nu^{\ddagger}$ appreciably possibly because of known limitations of DFT.[56−58] As long as state-specific gradients of multistate MCSCF wave functions of *solvated*


dx.doi.org/10.1021/ic5015785 | Inorg. Chem. 2014, 53, 9923−9931

systems are unavailable, the accuracy of $\nu^{\ddagger}$ obtained with LC-BOP cannot be assessed. The possibly underestimated, but nevertheless high, $\nu^{\ddagger}$ values obtained with LC-BOP arise from a strong coupling of nuclear and electronic motions: a small displacement of the atoms in the TS along the asymmetric $\nu^{\ddagger}$ mode gives rise to an asymmetric wave function. In the absence of CPCM hydration, both isomers of the P/S dissociate into monomers at the LC-BOP and the 4st-MCSCF levels. Realistic geometries of these highly charged systems can only be obtained if hydration effects are included.

The electronic coupling matrix element ($H_{ab}$) was computed via eq 7 with four-state-averaged XGMC-QDPT2 (abbreviated as 4st-XGMC-QDPT2) at geometries obtained with DFT (Table 2). At the TS (Figure 1), the difference of $E_b^{\ddagger} - E_a^{\ddagger}$ is equal to $E_{in,b}^{\ddagger} - E_{in,a}^{\ddagger}$ because states a and b exhibit equal hydration energies in a good approximation, since for both states, the electron is delocalized over the two metal centers. State b is the second state in which the antisymmetric MO of $d_{z^2}$ shape is populated. The corresponding 4st-XGMC-QDPT2 energies were evaluated for the respective CASSCF wave functions and two-ORMAS space MCSCF wave functions (see Computational Details). $H_{ab}$ does not depend on the excitation level because it is virtually equal for 4st-XGMC-QDPT2 based on either 4st-CASSCF(7/10) or 4st-MCSCF(6/6,1/4,7) wave functions (Table 2). For the linear TS structure, $H_{ab}$ is considerably larger. For the present inner-sphere electron-transfer reaction, $H_{ab}$ is much larger than for the outer-sphere self-exchange reactions of the $V(OH_2)_6^{2+/3+}$ and $Ru(OH_2)_6^{2+/3+}$ couples.[59]

**Table 2. Electronic Coupling Matrix Element ($H_{ab}$) and Internal Activation Energy ($\Delta E_{in}^{\ddagger}$) for the Transformation of the Precursor Complex into the TS[a]**

| | | | $\Delta E_{in}^{\ddagger}$ | |
|---|---|---|---|---|
| geometry/basis set | method (active space) | $H_{ab}$ | WFT | DFT |
| | (i) Bent Structure | | | |
| LC-BOP/sv(p) | 4st-XGMC-QDPT2 (6/6,1/4,7) | 34.0 | 43.1 | 27.0 |
| | 4st-XGMC-QDPT2 (7/10) | 33.0 | | |
| LC-BOP/svp | 4st-XGMC-QDPT2 (6/6,1/4,7) | 36.1 | 43.7 | 28.9 |
| LC-BOP/tzvp | 4st-XGMC-QDPT2 (6/6,1/4,7) | 36.1 | 53.3 | 35.2 |
| | 4st-XGMC-QDPT2 (7/10) | 35.2 | | |
| | (ii) Linear Structure | | | |
| LC-BOP/tzvp | 4st-XGMC-QDPT2 (6/6,1/4,7) | 56.0 | 55.7 | 42.4 |
| LC-BOP($\mu$=0.37)/tzvp | 4st-XGMC-QDPT2 (6/6,1/4,7) | 56.0 | 59.2 | 54.0 |
| | 4st-XGMC-QDPT2 (7/10) | 56.0 | | |

[a]Units of $H_{ab}$ and $\Delta E_{in}^{\ddagger}$: kJ mol$^{-1}$.

**Precursor/Successor Complex $(H_2O)_5Cr^{III}ClCr^{II}(OH_2)_5^{4+}$.** The bent and linear isomers of the P/S were obtained via the computation of the intrinsic reaction coordinate (IRC) represented in Figure 3. The sharp cusp is due to the relatively high imaginary frequency (Table 1). The electronic energy of the linear structure is insignificantly lower (by 2.6 kJ mol$^{-1}$) in contrast to $G$ being lower by 20.4 kJ mol$^{-1}$ (0 °C). Thus, the linear isomer is more stable because of its higher entropy. The electron to be or having been transferred is localized on the $Cr^{II}$

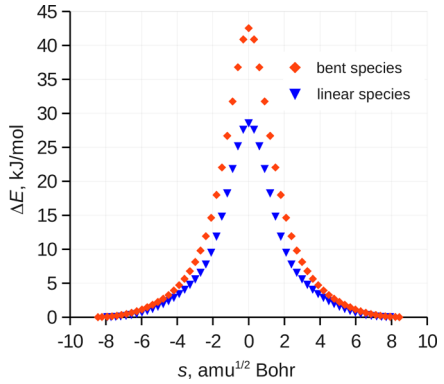


**Figure 3.** IRC of electron self-exchange reaction (3) [LC-BOP-($\mu$=0.33)-CPCM/tzvp calculations].

center in a $d_{\sigma}$* MO with $d_{z^2}$ shape (Figure 4). For the bent structure (Figure 4), the two hydrogen bonds between

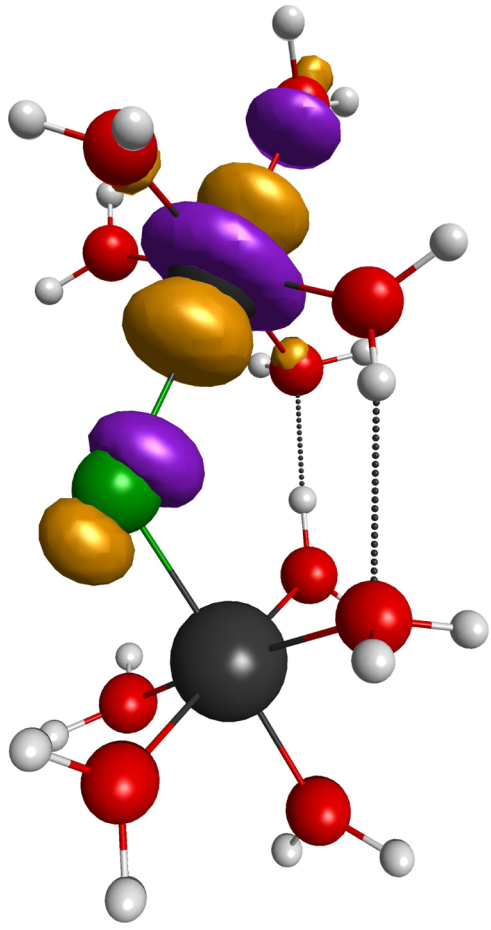

**Figure 4.** Structure of the bent P/S and MO of the electron being or having been transferred [LC-BOP($\mu$=0.33)-CPCM/tzvp calculation]. The colors have the same meanings as those in Figure 2.

equatorial water ligands remained unchanged during the IRC calculation. However, another bent isomer of the P/S exhibiting a slightly lower electronic energy (by 5.0 kJ mol$^{-1}$) but a higher Gibbs energy (by 4.7 kJ mol$^{-1}$ at 0 °C) exists in which two equatorial water ligands of $Cr^{III}$ are hydrogen-bond donors and two equatorial water ligands of $Cr^{II}$ hydrogen-bond acceptors (Figure S1 in the SI). It should be noted that a direct electron


dx.doi.org/10.1021/ic5015785 | Inorg. Chem. 2014, 53, 9923−9931

Table 3. Internal ($\lambda_{in}$), Outer-Sphere ($\lambda_{ou}$), and Total ($\lambda$) Reorganizational Energies Computed Based on the P/S Geometry[a]

| geometry/basis set | $d$(Cr···Cr), Å | $\lambda_{in}$[b] | $\lambda_{ou}$ eq 9 | $\lambda_{ou}$ eq 10[c] | $\lambda_{ou}$ eq 10[d] | $\lambda$ eqs 8a/9 | $\lambda$ eqs 8a/10[c] | $\lambda$ eqs 8a/10[d] |
|---|---|---|---|---|---|---|---|---|
| (i) Bent P/S Structure | | | | | | | | |
| LC-BOP($\mu$=0.33)/sv(p) | 4.364 | 306.45 | 48.73 | 45.69 | 64.09 | 355.18 | 352.14 | 370.54 |
| LC-BOP($\mu$=0.33)/svp | 4.385 | 312.74 | 49.73 | 43.72 | 61.89 | 362.47 | 356.46 | 374.63 |
| LC-BOP($\mu$=0.33)/tzvp | 4.452 | 325.67 | 52.21 | 29.43 | 46.91 | 377.88 | 355.10 | 372.58 |
| (ii) Linear P/S Structure | | | | | | | | |
| LC-BOP($\mu$=0.33)/tzvp | 5.193 | 320.08 | 76.63 | −55.69 | −29.47 | 396.71 | 264.39 | 290.61 |
| LC-BOP($\mu$=0.37)/tzvp | 5.226 | 331.22 | 77.57 | −68.00 | −43.87 | 408.79 | 263.22 | 287.34 |

[a]Units of $\lambda_{in}$, $\lambda_{ou}$, and $\lambda$: kJ mol$^{-1}$. [b]4st-XGMC-QDPT2(6/6,1/4,7). [c]$\Delta G_{solv}^{\ddagger}$ calculated with DFT. [d]$\Delta G_{solv}^{\ddagger}$ calculated with WFT.

Table 4. Activation Energies for the Electron-Transfer Step [Reaction (3)][a]

| geometry/basis set | $\Delta E^{\ddagger}$ (eqs 9 and 11) WFT[b] | $\Delta E^{\ddagger}$ (eqs 9 and 11) DFT | $\Delta E^{\ddagger}$ (eqs 10 and 11) WFT[b,c] | $\Delta E^{\ddagger}$ (eqs 10 and 11) DFT[c] | $\Delta E^{\ddagger}$ (eqs 10 and 11) WFT[b,d] | $\Delta E^{\ddagger}$[b] based on eqs 7, 8, 9, 12 | $\Delta E^{\ddagger}$[b] based on eqs 7, 8, 10, 12[c] | $\Delta E^{\ddagger}$[b] based on eqs 7, 8, 10, 12[d] | $\Delta G^{\ddagger}$(WFT)[b] based on eqs 10, 11[d] | $\Delta G^{\ddagger}$(WFT)[b] based on eqs 7, 8, 10, 12[d] |
|---|---|---|---|---|---|---|---|---|---|---|
| (i) Bent Structure | | | | | | | | | | |
| LC-BOP/sv(p) | 55.3 | 39.2 | 54.5 | 38.4 | 59.1 | 58.0 | 57.3 | 61.7 | 58.2 | 60.8 |
| LC-BOP/svp | 56.1 | 41.3 | 54.6 | 39.8 | 59.2 | 58.1 | 56.7 | 61.1 | 63.2 | 65.1 |
| LC-BOP/tzvp | 66.4 | 48.2 | 60.7 | 42.6 | 65.1 | 61.8 | 56.3 | 60.5 | 65.3 | 60.7 |
| (ii) Linear Structure | | | | | | | | | | |
| LC-BOP/tzvp | 74.9 | 61.6 | 41.8 | 28.5 | 48.4 | 51.1 | 22.0 | 27.5 | 56.1 | 35.2 |
| LC-BOP($\mu$=0.37)/tzvp | 78.6 | 73.4 | 42.2 | 37.0 | 48.3 | 53.9 | 21.7 | 26.8 | 59.5 | 38.0 |

[a]Units of $\Delta E^{\ddagger}$ and $\Delta G^{\ddagger}$: kJ mol$^{-1}$. [b]4st-XGMC-QDPT2(6/6,1/4,7). [c]$\Delta G_{solv}^{\ddagger}$ calculated with DFT. [d]$\Delta G_{solv}^{\ddagger}$ calculated with WFT.

self-exchange reaction via this isomer would give rise to an asymmetric TS, in which the two chromium centers would be inequivalent (two water ligands of one chromium center would be hydrogen-bond donors, whereas two water ligands of the other chromium would be hydrogen-bond acceptors). The subsequently formed successor complex (Figure S2 in the SI) exhibits a single hydrogen bond, whereby a water ligand bound to chromium(II) is a hydrogen-bond donor. Its electronic energy is significantly higher (by 22.0 kJ mol$^{-1}$) than that of its corresponding precursor complex (Figure S1 in the SI), but its Gibbs energy is marginally lower (by 2.2 kJ mol$^{-1}$ at 0 °C). The Gibbs energies of the three isomers of $(H_2O)_5Cr^{III}ClCr^{II}(OH_2)_5^{4+}$ (Figures 4 and S1 and S2 in the SI) are very close.

**Reorganizational Energy ($\lambda$).** The internal reorganizational energy $\lambda_{in}$ (Table 3) was calculated via eq 8b at the P/S geometry (Figure 1) using 4st-XGMC-QDPT2(6/6,1/4,7). $E_{in,b}$ corresponds to the third state, in which the $Cr^{III}$ MO with $d_{z^2}$ shape, being empty in the ground state, is occupied, and $E_{in,a}$ is the ground-state energy (with the $Cr^{II}$ MO exhibiting $d_{z^2}$ shape being occupied). In states 2 and 4, the MOs of $Cr^{II}$ and $Cr^{III}$ with $d_{x^2-y^2}$ shape are populated. $\lambda_{in}$ is approximately equal for the bent and linear isomers (Table 3). In contrast to Marcus' theory, $\lambda_{in}$ is based on adiabatic energies.

As was already mentioned, $\lambda_{ou}$ calculated according to eq 9[50−52] (details are given in the SI) is based on assumptions (Theoretical Basis) that are not necessarily fulfilled for inner-sphere electron-transfer reactions. In contrast, eq 10 is free of these suppositions but requires the structures of the TS and P/S, which are available in the present study. For the bent isomer, the $\lambda_{ou}$ values calculated using eqs 9 and 10 agree (Table 3i) because the Cr···Cr distance change is small for the transformation of the P/S into the TS. For such cases, eq 9 seems to be applicable in spite of the strong electronic interaction ($H_{ab}$; Table 2) and $r < r_{II} + r_{III}$ (Table S6 in the SI). $\Delta G_{solv}^{\ddagger}$ based on WFT is larger than the value calculated with DFT. For the linear isomer (Table 3ii), eqs 9 and 10 yielded considerably different $\lambda_{ou}$ values, whereby those based on eq 10 are negative. This is due to the large Cr···Cr distance reduction of almost 0.4 Å in the activation process (Tables 1ii and 3ii). The reduced Cr···Cr distance in the TS gives rise to a smaller molar volume of the TS and, therefore, a higher hydration energy, as predicted by the Born[60] model, for example. This higher hydration energy of the TS compared with that of the P/S is responsible for the negative $\lambda_{ou}$ value. The present results suggest that eq 9 is not applicable to systems involving a sizable metal−metal distance change during the activation process. As for the bent structure, $\Delta G_{solv}^{\ddagger}$ based on WFT is higher and, therefore, $\lambda_{ou}$ is higher by ∼25 kJ mol$^{-1}$. $\lambda_{ou}$ based on eq 9 (Table 3) is larger for the linear isomer because of its considerably longer Cr···Cr distance (by 0.74 Å).

**Electronic Activation Energy ($\Delta E^{\ddagger}$) and Gibbs Activation Energy ($\Delta G^{\ddagger}$) for the Electron-Transfer Step.** The internal (nuclear) activation energy ($\Delta E_{in}^{\ddagger}$) for the electron-transfer step [reaction (3)], $E_{in}^{\ddagger} - E_{in}$ ($=E_{in,a}^{\ddagger} - E_{in,a}$), was calculated based on the gas-phase electronic energies of the TS and P/S. The $\Delta E_{in}^{\ddagger}$ values calculated with DFT are lower than those of WFT (Table 2). This difference is minimal for the linear isomer computed with the nondefault $\mu$ parameter of 0.37. As was already mentioned, the bent isomer cannot be obtained with $\mu$ = 0.37; instead, the calculation converged toward the linear structure.

The (total) electronic activation energy ($\Delta E^{\ddagger}$) for the electron-transfer step [reaction (3)] can be obtained via eq 11 with $\Delta E_{in}^{\ddagger}$ calculated with DFT or WFT (Table 2) and $\lambda_{ou}$ evaluated using eq 9 or 10 (Table 3), whereby the hydration energy difference is available via DFT and WFT (Table 4). Alternatively, $\Delta E^{\ddagger}$ can be computed based on eq 12, with $\lambda$ calculated in various ways as described above.

The too low $\Delta E_{in}^{\ddagger}$ values obtained with DFT (Table 2) give rise to underestimated $\Delta E^{\ddagger}$ values (Table 4) apart from the exception of the LC-BOP($\mu$=0.37) data for the linear isomer.


dx.doi.org/10.1021/ic5015785 | Inorg. Chem. 2014, 53, 9923−9931

Table 5. Rate Constant for the Electron-Transfer Step ($k_{et}$) and the Electron Self-Exchange Reaction ($k$) of the $CrCl(OH_2)_5^{2+}/Cr(OH_2)_6^{2+}$ Couple at 0 °C and 1 M Ionic Strength[a]

| geometry | $\nu_n$,[b] $cm^{-1}$ | $\Delta G^{\ddagger}$,[c] kJ $mol^{-1}$ | $\Gamma_n$ | $\lambda$,[d] kJ $mol^{-1}$ | $H_{ab}$,[e] kJ $mol^{-1}$ | $\nu_{el}$, $s^{-1}$ | $k_{et}$, $s^{-1}$ | $k = K_A k_{et}$,[f] $M^{-1}$ $s^{-1}$ |
|---|---|---|---|---|---|---|---|---|
| (i) Bent Structure | | | | | | | | |
| LC-BOP($\mu$=0.33)/sv(p) | 568 | 58.2, 60.8 | 1.50 | 370.54 | 34.04 | $1.11 \times 10^{15}$ | 190, 60 | 6.7, 2.1 |
| LC-BOP($\mu$=0.33)/svp | 582 | 63.2, 65.1 | 1.53 | 374.63 | 36.06 | $1.24 \times 10^{15}$ | 22, 9.5 | 0.8, 0.3 |
| LC-BOP($\mu$=0.33)/tzvp | 627 | 65.3, 60.7 | 1.66 | 372.58 | 36.12 | $1.25 \times 10^{15}$ | 10.1, 77 | 0.4, 2.7 |
| (ii) Linear Structure | | | | | | | | |
| LC-BOP($\mu$=0.33)/tzvp | 460 | 56.1, 35.2 | 1.29 | 290.61 | 55.98 | $3.40 \times 10^{15}$ | 330, $3.3 \times 10^6$ | 12, $1.2 \times 10^5$ |
| LC-BOP($\mu$=0.37)/tzvp | 628 | 59.5, 38.0 | 1.66 | 287.35 | 55.98 | $3.42 \times 10^{15}$ | 131, $1.7 \times 10^6$ | 4.6, $6.0 \times 10^4$ |

[a] $\kappa_{el}$ = 1; see the text. [b] Data from Table 1. [c] Data from Table 4. [d] Data from Table 3. [e] Data from Table 2. [f] $K_A$ = 0.0354 $M^{-1}$; see the text.

For the bent structure, $\Delta E^{\ddagger}$ based on WFT does not depend on the equations for the calculation of $\lambda_{ou}$, eq 9 or 10, and $\Delta E^{\ddagger}$ itself, eq 11 or 12. For this structure, for which the Cr···Cr distance change along the activation process is small (<0.1 Å; Tables 1 and 3), consistent $\lambda_{ou}$ and $\Delta E^{\ddagger}$ values were obtained on the basis of all of the combinations of eqs 9−12. However, for the linear structure, the conditions for the calculation of $\Delta E^{\ddagger}$ based on eq 9 or 12 are not met and, consequently, $\Delta E^{\ddagger}$ is not correct.

As was already mentioned, for the linear isomer, eq 9 for $\lambda_{ou}$ is not applicable because of the sizable Cr···Cr distance reduction during the electron-transfer step. Equation 12 is based on the assumption that $H_{ab}$ is equal at the TS and P/S. $H_{ab}$ depends on the Cr···Cr distance. Hence, like eq 9, eq 12 is applicable if the Cr···Cr distance does not vary during the electron-transfer step. For the bent isomer, this condition is fulfilled. This is the reason why consistent $\Delta E^{\ddagger}$ values were obtained with any combination of eqs 9−12. For the linear isomer, with a sizable Cr···Cr distance reduction along the electron-transfer step, eqs 9 and 12 are not applicable. Thus, only the $\Delta E^{\ddagger}$ values (Table 4) based on eqs 10 and 11 are correct.

The computation of $k_{et}$ (eq 18) requires $\Delta G^{\ddagger}$ (eq 19), which was estimated by adding the zero-point-energy and thermal corrections ($\Delta g_{in}^{\ddagger}$) to $\Delta E^{\ddagger}$. $\Delta g_{in}^{\ddagger}$ was calculated with DFT at 0 °C for comparison with experiment.[6,8]

$$\Delta G^{\ddagger} = \Delta E^{\ddagger} + \Delta g_{in}^{\ddagger} \quad (19)$$

For the bent isomer, $\Delta g_{in}^{\ddagger}$ is small and, therefore, $\Delta G^{\ddagger} \approx \Delta E^{\ddagger}$ (Table 4). However, for the linear isomer, $\Delta G^{\ddagger}$ is greater than $\Delta E^{\ddagger}$ (by ~10 kJ $mol^{-1}$) because $\Delta S_{in}^{\ddagger}$ is more negative than that for the bent structure. It should be noted that $\Delta G^{\ddagger}$ based on eq 12 cannot be correct because the conditions for its application are not fulfilled.

**Rate Constant ($k_{et}$) for the Electron-Transfer Step.** Because the electronic frequency factor $\nu_{el}$ (eq 13) is greater than the nuclear frequency factor $\nu_n$ by more than 1 order of magnitude (Table 5), $\kappa_{el}$ (eq 14) is equal to 1. Thus, the rate constant for the electron-transfer step (eq 18) depends on $\nu_n$, $\Gamma_n$, and the Gibbs activation energy ($\Delta G^{\ddagger}$). The nuclear factors $\nu_n$ and $\Gamma_n$ were determined based on $\nu^{\ddagger}$ ($\nu_n = |\nu^{\ddagger}|$) of the hydrated TS and $\Delta G^{\ddagger}$ (Tables 1 and 4) as described. $\Gamma_n$ is somewhat greater than 1. For the bent isomer, $k_{et}$ lies in the range of 10−190 $s^{-1}$; it is not very sensitive to the various methods for the evaluation of $\Delta G^{\ddagger}$ (Table 4). In contrast, for the linear isomer, $k_{et}$ based on $\Delta G^{\ddagger}$ calculated via eqs 7, 8, 10, and 12 is incorrect and about 3 orders of magnitude larger than $\Delta G^{\ddagger}$ based on eqs 10 and 11 (Tables 4 and 5), whereby the latter value is approximately equal to that for the bent isomer. For comparison with the experimental rate constant[6,8] of reaction (4), the thermodynamics and kinetics for the formation of the precursor complex have to be investigated.

**Formation of the P Complex via Water Substitution at $Cr(OH_2)_6^{2+}$.** The P complex is formed via the substitution of a water ligand at $Cr(OH_2)_6^{2+}$ by $CrCl(OH_2)_5^{2+}$ [reactions (6) and (20)] within the IAR of these reactants.

$$Cr^{II}(OH_2)_6 \cdot Cr^{III}Cl(OH_2)_5^{4+} \rightarrow H_2O \cdot (H_2O)_5Cr^{II}ClCr^{III}(OH_2)_5^{4+} \quad (20)$$

It proceeds via the $I_d$ mechanism and the bent transition state $(H_2O)_5Cr\cdots(OH_2)[ClCr(OH_2)_5]^{4+\ddagger}$ ($I_d$-TS). A weakly bound water ligand in $Cr(OH_2)_6^{2+}$ is displaced by the chloro ligand of $CrCl(OH_2)_5^{2+}$ in an adjacent attack[61] (Figure 5), which leads to a water adduct of the bent precursor complex. All of the attempts to compute the corresponding linear TS failed.

IRC calculations did not yield the IAR and the water adduct of the P/S (P/S·aq) in their lowest-energy configurations. By the rearrangement or addition of hydrogen bonds, species with lower energies were obtained. The question remains open as to whether they are in the global minimum, but it will be shown that, in the present context, this is not relevant. The P/S·aq has a lower Gibbs energy (by 9.7 kJ $mol^{-1}$) than the IAR because of its smaller molar volume, giving rise to a higher hydration energy. The rate constant ($k_{sub}$) for the substitution process [reaction (20)], calculated via Eyring's equation[62] for 0 °C ($\Delta G^{\ddagger}$ = 18.8 kJ $mol^{-1}$), $1.4 \times 10^9$ $s^{-1}$, is more than 6 orders of magnitude faster than $k_{et}$. Even if an IAR with a lower energy existed, the electron-transfer step would remain rate-determining.

**Calculated Rate Constant for the Electron Self-Exchange Reaction of the $CrCl(OH_2)_6^{2+}/Cr(OH_2)_6^{2+}$ Couple [Reaction (4)].** The observed rate constants ($k$) for reaction (4) at 0 °C and 1 M ionic strength are 8.3 ± 2.0 and 9.1 ± 1.0 $M^{-1}$ $s^{-1}$.[6,8] The first step of reaction (4), reaction (5), is the formation of the IAR. The corresponding equilibrium constant ($K_A$) at the experimental conditions was calculated based on Fuoss' equation.[28] As the distance between the two cations, the computed Cr···Cr distance of 5.081 Å in the IAR was taken. Hence, a value of 0.0354 $M^{-1}$ was obtained for $K_A$ (at 0 °C and 1 M ionic strength).

The second step of reaction (4), reaction (6) or (20), involving the substitution process, is much faster than electron transfer ($k_{sub} \gg k_{et}$). Possibly, it is followed by the rearrangement of P, the formation of the linear isomer, or the rearrangement of hydrogen bonds, for example. In a third stage, the electron is transferred [reaction (3)] at a rate of $k_{et}$. Because the latter is rate-determining, the rate constant of reaction (4) ($k$) is equal to $K_A k_{et}$.


dx.doi.org/10.1021/ic5015785 | Inorg. Chem. 2014, 53, 9923−9931

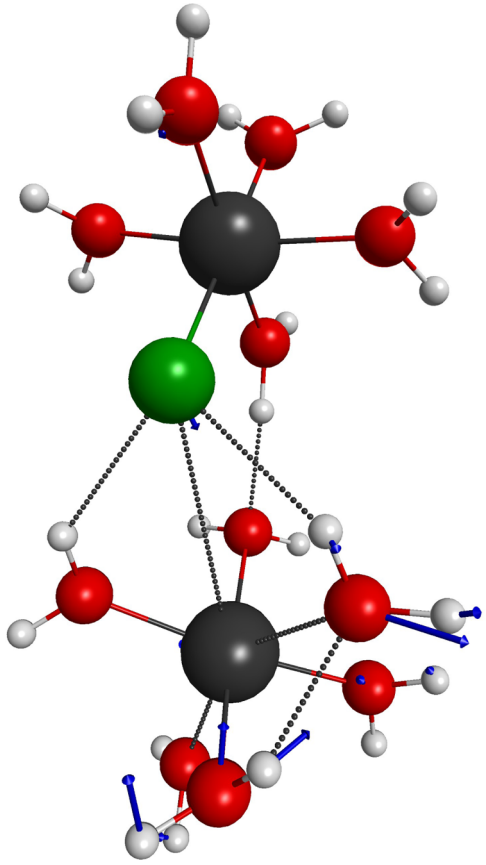

**Figure 5.** Structure of the TS for water substitution at $Cr(OH_2)_6^{2+}$ by $CrCl(OH_2)_5^{2+}$, $(H_2O)_5Cr\cdots(OH_2)[ClCr(OH_2)_5]^{4+\ddagger}$ ($I_d$-TS), with imaginary mode [LC-BOP($\mu$=0.33)-CPCM/tzvp calculation]. The colors have the same meanings as those in Figure 2

The calculated $k$ values (Table 5) agree with experiment within the error limits, except the two values for the linear isomer, for which $\Delta G^{\ddagger}$ was calculated based on eqs 7, 8, 10, and 12. This is expected because eq 12 is not applicable for reactions involving sizable changes of the metal−metal distance during the electron-transfer step (the P → TS → S transformation) as discussed above. Thus, the results for the linear isomer based on eq 12 should be disregarded. $k$ computed for the bent and linear structures are virtually equal, suggesting that reaction (4) could proceed via both structures.

**PESs of Inner-Sphere Electron-Transfer Reactions.** In reaction (4), the substitution process leading to P (reaction 6) and the electron-transfer step [reaction (3)] proceed in two distinct reactions. Thus, the P and S are local minima on the PES (Figure 1), and the calculation of $\lambda$, $H_{ab}$, $\nu^{\ddagger}$, $\Delta E^{\ddagger}$, and $\Delta G^{\ddagger}$ is straightforward. However, the P and S are not necessarily local minima on the PES because electron transfer might take place concerted with the substitution process, whereby either the latter or electron transfer could be rate-determining. In such cases, the computation of all of the above-mentioned parameters may not be possible.

**Summary.** This study shows why the inner-sphere pathway is much faster than the outer-sphere one. Compared with the outer-sphere self-exchange reaction of the $Cr(OH_2)_6^{2+/3+}$ couple,[5] the $Cl^-$-bridged inner-sphere reaction of the $CrCl(H_2O)_5^{2+}/Cr(OH_2)_6^{2+}$ couple is more than 5 orders of magnitude faster for the following reasons:

(i) The calculated value of $H_{ab}$, ~33−36 and ~56 kJ mol$^{-1}$ for the bent and linear TS, respectively, is much larger than that for the outer-sphere pathway [for the $V(OH_2)_6^{2+/3+}$ and $Ru(OH_2)_6^{2+/3+}$ couples, $H_{ab}$ is in the range of 0.1−0.2 kJ mol$^{-1}$ [59]]. The large $H_{ab}$ value lowers the hypothetical diabatic activation energy (the energy at the intersection of $E_\alpha$ and $E_\beta$ in Figure 1) substantially (by roughly $H_{ab}$). Furthermore, it gives rise to a large $\nu_{el}$, being greater than $\nu_n$, and, therefore, $\kappa_{el}$ is equal to 1 (for the $V(OH_2)_6^{2+/3+}$ and $Ru(OH_2)_6^{2+/3+}$ couples, $\kappa_{el}$ is less than $10^{-2}$ [59]). The large $H_{ab}$ value could account for the rate acceleration of a factor of ~$10^6$ compared with the outer-sphere pathway.

(ii) $\nu_n$ might be much larger than estimated on the basis of $Cr^{II}$−Cl and $Cr^{III}$−Cl stretching frequencies and thus augments $k_{et}$ because it is a factor in eq 18. Furthermore, the large $\nu_n$ value would give rise to a nuclear tunneling factor of greater than 1; in this case, $\Gamma_n$ ~ 1.3−1.7.

For this self-exchange reaction, P and S complexes exist for the bent and linear isomers (they represent local minima on the PES). The choice of the functional for the computation of the P/S geometry is not critical, but consistent properties for the TS were only obtained with long-range-corrected functionals; others produced a symmetry-broken wave function or a TS with a too low energy and imaginary mode, or the symmetric species was in a local minimum of the PES (without imaginary frequency).

Marcus' formula for the outer-sphere reorganizational energy $\lambda_{ou}$ (eq 9) and Brunschwig, Creutz, and Sutin's equation for the activation energy (eq 12) are based on the hypothesis that the donor−acceptor distance is constant during the electron-transfer step. In cases like that of the linear isomer, this condition is not fulfilled and, hence, these equations are not applicable. A reduction of the donor−acceptor distance along the activation process can give rise to a negative outer-sphere reorganizational energy because of the smaller molar volume of the TS, exhibiting a higher (more negative) hydration energy. Furthermore, $H_{ab}$ at the TS is greater than that at the P/S.

## ■ ASSOCIATED CONTENT

### Supporting Information

Modified Karlsruhe basis sets and the procedure for their calculation, figure or atomic coordinates of the TS, P/S, IAR, $I_d$-TS, and P/S·aq species, and details on the calculation of $\lambda_{ou}$. This material is available free of charge via the Internet at http://pubs.acs.org.

## ■ AUTHOR INFORMATION


### Corresponding Author

*E-mail: francois.rotzinger@epfl.ch.


### Notes

The authors declare no competing financial interest.

## ■ ACKNOWLEDGMENTS

Prof. J. F. Endicott, Prof. H. B. Schlegel, and Dr. B. F. E. Curchod contributed helpful comments to the manuscript. The reviewers are acknowledged for their helpful and constructive criticism.

## ■ REFERENCES

(1) Taube, H.; Myers, H.; Rich, R. L. *J. Am. Chem. Soc.* **1953**, *75*, 4118.
(2) Taube, H. *Can. J. Chem.* **1959**, *37*, 129.

(3) Taube, H. *Electron Transfer Reactions of Complex Ions in Solution*; Academic Press: New York, 1970.
(4) Silverman, J.; Dodson, R. W. *J. Phys. Chem.* **1952**, *56*, 846.
(5) Anderson, A.; Bonner, N. A. *J. Am. Chem. Soc.* **1954**, *76*, 3826.
(6) Taube, H.; King, E. L. *J. Am. Chem. Soc.* **1954**, *76*, 4053.
(7) Krishnamurty, K. V.; Wahl, A. C. *J. Am. Chem. Soc.* **1958**, *80*, 5921.
(8) Ball, D. L.; King, E. L. *J. Am. Chem. Soc.* **1958**, *80*, 1091.
(9) Snellgrove, R.; King, E. L. *Inorg. Chem.* **1964**, *3*, 288.
(10) Bonner, N. A.; Hunt, J. P. *J. Am. Chem. Soc.* **1960**, *82*, 3826.
(11) Habib, H. S.; Hunt, J. P. *J. Am. Chem. Soc.* **1966**, *88*, 1668.
(12) Hudis, J.; Wahl, A. C. *J. Am. Chem. Soc.* **1953**, *75*, 4153.
(13) Hudis, J.; Dodson, R. W. *J. Am. Chem. Soc.* **1956**, *78*, 911.
(14) Proll, P. J. In *Comprehensive Chemical Kinetics*; Bamford, C. H., Tipper, C. F. H., Eds.; Elsevier: Amsterdam, The Netherlands, 1972; Vol. *7*, p 56.
(15) Marcus, R. A. *Discuss. Faraday Soc.* **1960**, *29*, 21.
(16) Hush, N. S. *Trans. Faraday Soc.* **1961**, *57*, 557.
(17) Levich, V. G.; Dogonadze, R. R.; Kuznetsov, A. M. *Electrochim. Acta* **1968**, *13*, 1025.
(18) Brunschwig, B. S.; Logan, J.; Newton, M. D.; Sutin, N. *J. Am. Chem. Soc.* **1980**, *102*, 5798.
(19) Sutin, N. *Prog. Inorg. Chem.* **1983**, *30*, 441.
(20) Newton, M. D.; Sutin, N. *Annu. Rev. Phys. Chem.* **1984**, *35*, 437.
(21) Marcus, R. A.; Sutin, N. *Biochim. Biophys. Acta* **1985**, *811*, 265.
(22) Newton, M. D. *Chem. Rev.* **1991**, *91*, 767.
(23) Brunschwig, B. S.; Sutin, N. *Coord. Chem. Rev.* **1999**, *187*, 233.
(24) Brunschwig, B. S.; Creutz, C.; Sutin, N. *Chem. Soc. Rev.* **2002**, *31*, 168.
(25) Freed, K. F.; Jortner, J. *J. Chem. Phys.* **1970**, *52*, 6272.
(26) Kestner, N. R.; Logan, J.; Jortner, J. *J. Phys. Chem.* **1974**, *78*, 2148.
(27) *Electron Transfer in Chemistry*; Balzani, V., Ed.; Wiley-VCH: Weinheim, Germany, 2001; Vols. *1*−*5*.
(28) Fuoss, R. M. *J. Am. Chem. Soc.* **1958**, *80*, 5059.
(29) Schmidt, M. W.; Baldridge, K. K.; Boatz, J. A.; Elbert, S. T.; Gordon, M. S.; Jensen, J. H.; Koseki, S.; Matsunaga, N.; Nguyen, K. A.; Su, S. J.; Windus, T. L.; Dupuis, M.; Montgomery, J. A. *J. Comput. Chem.* **1993**, *14*, 1347.
(30) Gordon, M. S.; Schmidt, M. W. In *Theory and Applications of Computational Chemistry: The First Forty Years*; Dykstra, C. E., Frenking, G., Kim, K. S., Scuseria, G. E., Eds.; Elsevier: Amsterdam, The Netherlands, 2005; p 1167.
(31) Schäfer, A.; Horn, H.; Ahlrichs, R. *J. Chem. Phys.* **1992**, *97*, 2571.
(32) Schäfer, A.; Huber, C.; Ahlrichs, R. *J. Chem. Chem.* **1994**, *100*, 5829.
(33) Weigend, F.; Ahlrichs, R. *Phys. Chem. Chem. Phys.* **2005**, *7*, 3297.
(34) Bode, B. M.; Gordon, M. S. *J. Mol. Graphics Modell.* **1998**, *16*, 133.
(35) Ivanic, J. *J. Chem. Phys.* **2003**, *119*, 9364.
(36) Nakano, H.; Uchiyama, R.; Hirao, K. *J. Comput. Chem.* **2002**, *23*, 1166.
(37) Miyajima, M.; Watanabe, Y.; Nakano, H. *J. Chem. Phys.* **2006**, *124*, 044101.
(38) Ebisuzaki, R.; Watanabe, Y.; Nakano, H. *Chem. Phys. Lett.* **2007**, *442*, 164.
(39) Roskop, L.; Gordon, M. S. *J. Chem. Phys.* **2011**, *135*, 044101.
(40) Granovsky, A. A. *J. Chem. Phys.* **2011**, *134*, 214113.
(41) Tomasi, J. *Theor. Chem. Acc.* **2004**, *112*, 184.
(42) Tomasi, J.; Mennucci, B.; Cammi, R. *Chem. Rev.* **2005**, *105*, 2999.
(43) Barone, V.; Cossi, M. *J. Phys. Chem. A* **1998**, *102*, 1995.
(44) Batsanov, S. S. *Inorg. Mater.* **2001**, *37*, 871.
(45) Miller, W. H.; Handy, N. C.; Adams, J. E. *J. Chem. Phys.* **1980**, *72*, 99.
(46) Nakamura, H.; Truhlar, D. G. *J. Chem. Phys.* **2001**, *115*, 10353.
(47) Nakamura, H.; Truhlar, D. G. *J. Chem. Phys.* **2002**, *117*, 5576.
(48) Nakamura, H.; Truhlar, D. G. *J. Chem. Phys.* **2003**, *118*, 6816.
(49) Yang, K. R.; Xu, X.; Truhlar, D. G. *Chem. Phys. Lett.* **2013**, *573*, 84.
(50) Marcus, R. A. *J. Chem. Phys.* **1956**, *24*, 966.
(51) Marcus, R. A. *J. Chem. Phys.* **1957**, *26*, 867.
(52) Marcus, R. A. *J. Chem. Phys.* **1957**, *26*, 872.
(53) Skodje, R. T.; Truhlar, D. G. *J. Phys. Chem.* **1981**, *85*, 624.
(54) Tawada, Y.; Tsuneda, T.; Yanagisawa, S.; Yanai, Y.; Hirao, K. *J. Chem. Phys.* **2004**, *120*, 8425.
(55) Logan, J.; Newton, M. D. *J. Chem. Phys.* **1983**, *78*, 4086.
(56) Cohen, A. J.; Mori-Sánchez, P.; Yang, W. *Science* **2008**, *321*, 792.
(57) Becke, A. D. *J. Chem. Phys.* **2013**, *139*, 021104.
(58) Johnson, E. R. *J. Chem. Phys.* **2013**, *139*, 074110.
(59) Rotzinger, F. P. *Dalton Trans.* **2002**, 719.
(60) Born, M. Z. *Physik* **1920**, *1*, 45.
(61) Rotzinger, F. P. *Chem. Rev.* **2005**, *105*, 2003.
(62) Eyring, H. *J. Chem. Phys.* **1935**, *35*, 107.


dx.doi.org/10.1021/ic5015785 | *Inorg. Chem.* 2014, 53, 9923−9931